# Graphene Nanoelectrodes: Fabrication and Size-Dependent Electrochemistry

Bo Zhang, Lixin Fan, Huawei Zhong, Yuwen Liu, and Shengli Chen*

Key Laboratory of Analytical Chemistry for Biology and Medicine (Ministry of Education), Hubei Key Laboratory of Electrochemical Power Sources, Department of Chemistry, Wuhan University, Wuhan, People's Republic of China

S Supporting Information

ABSTRACT: The fabrication and electrochemistry of a new class of graphene electrodes are presented. Through high-temperature annealing of hydrazine-reduced graphene oxides followed by high-speed centrifugation and size-selected ultra-filtration, flakes of reduced graphene oxides (r-GOs) of nanometer and submicrometer dimensions, respectively, are obtained and separated from the larger ones. Using n-dodecanethiol-modified Au ultramicroelectrodes of appropriately small sizes, quick dipping in dilute suspensions of these small r-GOs allows attachment of only a single flake on the thiol monolayer. The electrodes thus fabricated are used to study the heterogeneous electron transfer (ET) kinetics at r-GOs and the nanoscopic charge transport dynamics at electrochemical interfaces. The r-GOs are found to exhibit similarly high activity for electrochemical ET reactions to metal electrodes. Voltammetric analysis for the relatively slow ET reaction of $Fe(CN)_6^{3-}$ reduction produces slightly higher ET rate constants at r-GOs of nanometer sizes than at large ones. These ET kinetic features are in accordance with the defect-dominant nature of the r-GOs and the increased defect density in the nanometer-sized flakes as revealed by Raman spectroscopic measurements. The voltammetric enhancement and inhibition for the reduction of $Ru(NH_3)_6^{3+}$ and $Fe(CN)_6^{3-}$, respectively, at r-GO flakes of submicrometer and nanometer dimensions upon removal of supporting electrolyte are found to significantly deviate in magnitude from those predicted by the electroneutrality-based electromigration theory, which may evidence the increased penetration of the diffuse double layer into the mass transport layer at nanoscopic electrochemical interfaces.
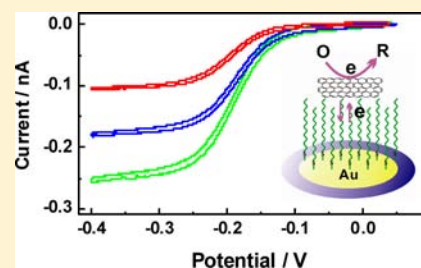
1. INTRODUCTION

As the newest member in the carbon family, graphenes are attracting increasing research interest. Electrochemistry is a particular area in which graphenes have both fundamental and applied significance.[1] On one hand, various novel carbons are always among the electrochemical focuses due to their unique surface chemistry and electronic structures.[2,3] Besides, the promise of graphenes in constructing high performance electrodes for ultracapacitors,[4] fuel cells,[5] and batteries[6] requires knowledge of their charge storage and transfer properties.

Chemical-vapor-deposition (CVD) is most capable of producing large area single/few layer of graphenes.[7] The fabrication of CVD graphene electrodes, however, mostly involves cumbersome sheet transfer and photolithographic processes,[8,9] which not only limit the widespread studies of graphene electrochemistry, but could also result in electrode contamination and even damage.[10] Reduced graphene oxides (r-GOs), which can be generated more facilely and scalably,[11] represent another common form of graphenes and are most widely used in various electrochemical energy technologies.[4,5c,6] Currently, r-GO-based electrodes, in either fundamental or applied studies, are mostly prepared as relatively thick films on conducting substrates through drop casting,[12] adsorption with self-assembled-monolayer (SAM),[13] in situ electrochemical reduction, and other methods.[14] The involvement of r-GO

sheets of diverse shapes and dimensions and the uncontrolled porosity and accessibility of the electroactive surface areas in the films make the measurements of intrinsic electrochemical properties of graphenes difficult.

In this study, we introduce a type of graphene electrode in which a single r-GO sheet is immobilized on alkylthiol-modified Au electrodes. Our strategy is to separate r-GOs into flakes of different size ranges and use SAM-modified Au ultra-microelectrodes (UME) of appropriately small sizes as substrates to attach flakes of certain size ranges in dilute suspensions, which can effectively reduce the possibility of multiflake immobilization.

The SAMs in most cases form a compact and rigid film,[15] which can therefore block the electron transfer (ET) of Au with redox molecules attached on its end or in solution due to the long distance effect.[16] However, efficient electron tunneling can take place between Au and the immobilized conducting materials, such as metal nanoparticles, carbon nanotubes, and graphenes,[13,17] mainly because they have much higher density of states than the redox molecules. An excellent analysis on this can be found in recent literature by Chazalviel et al.[17a] Thus, the voltammetric responses of the present r-GO electrodes

would be predominantly determined by the interfacial electrochemical processes at the immobilized single r-GO flakes.

In addition to providing a way to study the intrinsic electrochemistry of individual r-GO sheets, the present approach also offers a straightforward alternative to fabricate planar carbon electrodes of submicrometer and nanometer dimensions, which are appreciated due to their capability of probing fast heterogeneous ET kinetics[18,19] and nanoscopic charge transport dynamics.[20−24] Currently, such small electrodes are usually fabricated by shielding thinned metal/carbon wires with glasses[18c,d,19] or polymers,[18a,b,25] which could lead to electrode recession and insulation defects.[19c,21a,b,26]

2. EXPERIMENTAL SECTION

Chemicals, apparatus, and measurement details are given in the Supporting Information (SI, sections 1 and 2).

2.1. Preparation of r-GOs. The GOs were prepared according to the modified Hummers method[5c,27] (SI, section 3). The r-GOs were prepared by using a combined chemical and thermal reduction of GOs.[28,29] Briefly, the r-GO sample was first dispersed in doubly distilled water to give a colloidal solution, into which the hydrazine hydrate was added. The resulting mixture was kept at 80 °C for 12 h under ultrasonication and was then centrifuged and washed with deionized water repeatedly. After being thoroughly rinsed, the chemically reduced GO product was annealed at 900 °C under Ar gas for ca. 30 min, which is believed to be able to reduce the oxygenated functional groups that cannot be effectively reduced by hydrazine and to repair some defects.[29]

2.2. Preparation of Size-Selected r-GO Suspensions. To prepare size-selected r-GO suspensions, the r-GO sample obtained from thermal annealing was subjected to a size fractionation process involving high-speed centrifugation and successive ultrafiltration (Scheme 1). First, 10 mg r-GOs were dispersed in 100 mL DMF

Scheme 1. Illustration of Electrode Fabrication

and vigorously disrupted under ultrasound for 15 min. The dispersion was then subjected to high-speed centrifugation under 16 600 rpm for 3 min, which resulted in sedimentation of roughly 80 wt % of the original sample and transformation of the dispersion color from black into faint black. The upper supernatant, which should contain single- and few-layer r-GO flakes of relatively small sizes, was then collected and filtered successively by using ultrafiltration membranes of 800, 450, and 220 nm pore sizes, respectively. The retained solid in each filtration was dispersed in 100 mL DMF to form a nearly colorless dispersion, which was further diluted by spreading 1 mL dispersion into 100 mL DMF. In result, four types of dilute r-GO suspensions, containing mainly r-GO flakes of <220 nm (I), 220−450 nm (II), 450−800 nm (III), and >800 nm (IV), respectively, were obtained. These suspensions were allowed to stand for a period of time to form a supernatant liquor for fabricating graphene electrodes.

2.3. Fabrication of Graphene Electrodes. The general strategy for electrode fabrication is depicted in Scheme 1. It was started with Au disk electrodes of micrometer and/or submicrometer dimensions prepared by laser-assisted pulling of annealed Au wires of 20 μm diameters in borosilicate capillaries (Drummond, 1.0-mm o.d., 0.2-mm i.d.) under vacuum with the help of a Sutter P-2000/G pipet

puller.[19,30] The exposure of Au disks were controlled by carefully polishing with 0.05 μm alumina powders and monitored with the voltammetry for the reduction of 10 mM Ru(NH$_3$)$_6^{3+}$ in 1 M KCl. Only Au electrodes larger than 0.5 μm in diameter were used in following steps to reduce the risk of electrode recession.

SAM-modified Au (Au/SAM) electrodes were formed by soaking Au disk electrodes in C$_{12}$H$_{25}$SH solution for at least 48 h at room temperature. Prior to use, the bare Au electrodes were ultrasonicated in ethanol and ultrapure water, respectively, for 3 min and then cleaned in Piranha solution (30% H$_2$O$_2$/concentrated H$_2$SO$_4$, 1:3 v/v). They were electrochemically polished by consecutive potential cycling between −0.40 and 0.9 V (Hg/Hg$_2$SO$_4$) at 0.05 V/s in 0.5 M H$_2$SO$_4$ until a characteristic cyclic voltammogram of a clean Au surface was obtained.

Immobilization of r-GO flakes was achieved by quick dipping of Au/SAM electrodes in r-GO suspensions described above. After rinsed with ultrapure water, the electrode was moved into an electrochemical cell containing a solution of 10 mM Ru(NH$_3$)$_6^{3+}$ in 1 M KCl to check whether the electrode gave a reduction wave not seen on the Au/SAM electrode. If not, further quick dipping was performed until the attachment of an r-GO flake. The electrodes thus prepared are denoted as graphene electrodes in the following.

3. RESULTS AND DISCUSSION

3.1. Electrode Fabrication and Characterization. Figure 1 displays the steady-state voltammetric responses of an Au/
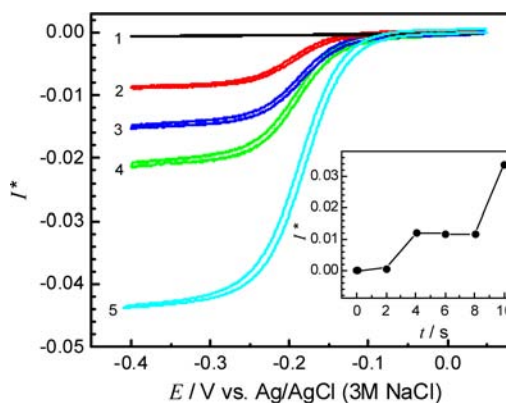

Figure 1. Voltammetric responses of a Au/SAM electrode (curve 1) and four graphene electrodes (curves 2−5) in the solution of 1 M KCl containing 10 mM Ru(NH$_3$)$_6^{3+}$. Potential scanning rate: 10 mV/s. Inset: limiting current variation in a multidipping experiment (see text for details). Currents are given in dimensionless form.

SAM electrode (curve 1) and graphene electrodes prepared by quick dipping in r-GO suspensions I (curves 2−4) and II (curve 5), respectively, for the reduction of 10 mM Ru(NH$_3$)$_6^{3+}$ in 1 M KCl. The diameters of the Au disks in these electrodes were ca. 0.5 μm (curves 1−4) and 1 μm (curve 5), respectively. For illustration purposes, the currents in Figure 1 have been normalized by the limiting current obtained on a bare Au disk electrode of 10 μm diameter in the same solution. In this way, the dimensionless limiting current (I_{dL}*) in each polarization curve could be a rough measure of the size of r-GO flake in the graphene electrode. If we assume that the flake has a disk shape, then an effective diameter can be estimated according to $d = 10 \times I_{dL}$* (μm).

As indicated by the almost negligible voltammetric current in curve 1, the C$_{12}$H$_{25}$SH SAM nearly completely inhibited the ET between the Au electrode and Ru(NH$_3$)$_6^{3+}$ in solution. The enlarged plot of curve 1 (Figure S1 of the SI) exhibited a much

lagged variation of current with potential, which further suggested a strong inhibition of the ET kinetics by SAM.

We also ran blank experiments by immersing Au/SAM electrodes in DMF without r-GOs for a few hours. The as-treated Au/SAM electrodes gave almost identical responses to the untreated ones. Thus, the voltammetric responses in curves 2−5 should be due to the reduction of $Ru(NH_3)_6^{3+}$ at the attached r-GO flakes, rather than through pinholes in SAMs formed during dipping experiments. It is known that the formation of alkanethiol SAMs usually undergoes a crystal-lization step and leads to a compact and rigid structure due to the strong Au−S bonding interaction and the strong hydro-phobic interaction among the long alkyl chains. The SAM is able to keep its integrity unless under extreme conditions, such as very positive potentials or high temperatures.[15]

To ensure that only a single r-GO flake is attached on each prepared electrode, we mainly used Au disk electrodes of submicrometer diameter ($<1~\mu$m) to attach r-GO flakes in suspension I, and that 1−2 μm in diameters to attach r-GO flakes in suspensions II and III. In addition, the concentrations of the r-GO suspensions were controlled to be very dilute (see section 2.2) and the dipping times of Au/SAM electrodes in the suspensions were controlled to be very short (typically less than 5 s).

Under such conditions, the attachment of an r-GO flake was found to be somewhat random in nature. In most cases, several times of dipping were required for successfully attaching an r-GO flake. The inset of Figure 1 shows the variation of the limiting current given by an Au/SAM electrode of ∼0.8 μm diameter in a multidipping experiment using suspension I, with the dipping and voltammetric measurement performed alternatively. In this experiment, the attachment of the first r-GO flake occurred in the second dipping. Upon further three times of dipping, the second r-GO flake was attached. Unless stated otherwise, graphene electrodes described in the following refer to those only the first attachment of r-GO flake was seen.

The random nature of the r-GO attachment was also indicated by the varied limiting currents, which represented the sizes of the attached r-GO flakes, in different dipping in the same suspension (Figure 1, curves 2−4). However, the effective diameters of the r-GO flakes estimated from $I_{dL}*$ roughly fell into the size range for each suspension. This indicated that the r-GOs were effectively separated into different size ranges in the size-selected filtration process, and that in most cases, only a single r-GO was attached in each dipping. AFM images of r-GO flakes from different suspensions (Figure 2) also indicated that their sizes were approximately within the expected ranges.

Due to the fact that the surface roughness of Au substrates was beyond the thicknesses of the SAMs and the attached r-GO flakes, and that the SAM could respond elastically to AFM tips, it was difficult to image r-GO flakes on Au/SAM electrodes. AFM images obtained on cleaved mica surfaces through drop casting of the dilute suspensions showed that the prepared r-GO flakes were considerably diverse and irregular in shape (Figure 2a−c). In general, the larger flakes looked more round, and the smaller ones were more flat. Interestingly, the smallest flakes in suspension I were found to be predominantly shaped in short ribbons of low aspect ratios (Figure 2a), which was also indicated by the TEM images (Figure S2 of the SI). The lengths and widths of these small r-GOs were typically 130−180 nm and 40−90 nm, respectively. It seems that very small r-GO flakes derived from high temperature annealing tend to have narrow flat geommetries.[31]
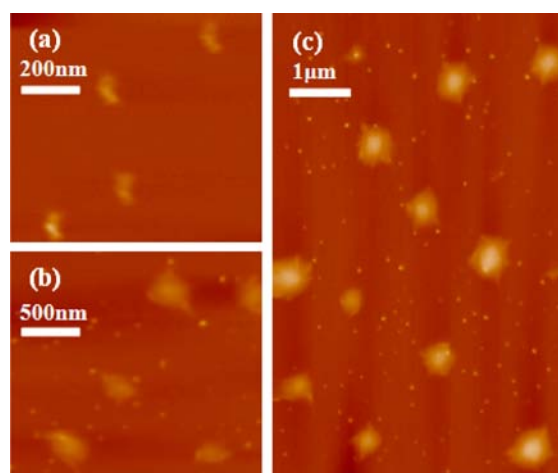

Figure 2. Representative AFM images of r-GO flakes in suspensions (a) I, (b) II, and (c) III obtained under a tapping mode of 1024 × 1024 pixel resolution on mica surfaces.

The AFM topographic heights of the r-GO flakes on mica surfaces were mostly in the range of 1−3 nm (Figures S3 and S4 of the SI), which can be ascribed to single- and/or few-layer r-GO sheets when considering the intrinsic wrinkles of r-GOs and the adsorption of solvent molecules on them.[32] Due to the fact that the r-GOs could undergo restacking in the course of drop-casting due to the hydrophobic interaction, and that the mica surface is very different from SAMs in roughness and charge, the AFM geometric information obtained on a mica surface might not represent the real layer numbers and the exact shapes of the r-GO flakes in suspensions and on electrodes. By employing very dilute suspensions and quick dipping procedures, we expect that the aggregation and restacking could be greatly inhibited in the prepared electrodes.

In addition to r-GO flakes, some dot-like structures were also observed in the AFM images, which should be the assemblies of solvent molecules since they also appeared on mica surface after drop casting of r-GO free DMF (Figure S5 of the SI). Similar dot structures were also seen in AFM images of graphenes by others.[33] By purposely choosing small sampling areas, these structures can be excluded when imaging the small r-GO flakes (Figure 2a).

3.2. Heterogeneous ET Kinetics at r-GO Flakes. The heterogeneous ET kinetics at graphene-based materials is not only intrinsic to their electrochemical applications, but is also fundamentally important in understanding the relation between ET kinetics and the electronic structures of electrode materials.[8a,34−36] We used $Ru(NH_3)_6^{3+}$ and $Fe(CN)_6^{3-}$, two commonly used redox probes with relatively fast and slow ET kinetics, respectively, to probe the heterogeneous ET kinetics at r-GOs.

Figure 3 shows the variation of the half-wave potentials ($E_{1/2}$) as functions of $I_{dL}*$ on the steady-state polarization curves for the reduction of the two redox probes on r-GO flakes of various sizes. The $E_{1/2}$ was given with respect to that obtained on the 10 μm Au electrode, at which the two reactions were nearly reversible and therefore the half-wave potentials can be approximately considered the formal potentials (E^0).[37,38] It should be mentioned that we used the negative going branches in the cyclic voltammograms (CVs) obtained under a potential scanning rate of 10 mV/s as the polarization curves for kinetic analysis, with the double layer charging background
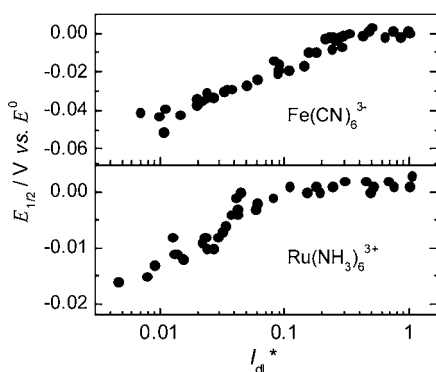
Figure 3. Plots of half-wave potentials as functions of limiting currents on the steady-state polarization curves for the reduction of 10 mM $Fe(CN)_6^{3-}$ and $Ru(NH_3)_6^{3+}$ in 1 M KCl on graphene electrodes of differently sized r-GO flakes.

Figure 4. Fitting examples of the polarization curves obtained on graphene electrodes prepared from suspensions I ($d \approx 140$ nm) and II ($d \approx 326$ nm), respectively, for the reduction of 10 mM $Fe(CN)_6^{3-}$ in 1 M KCl.
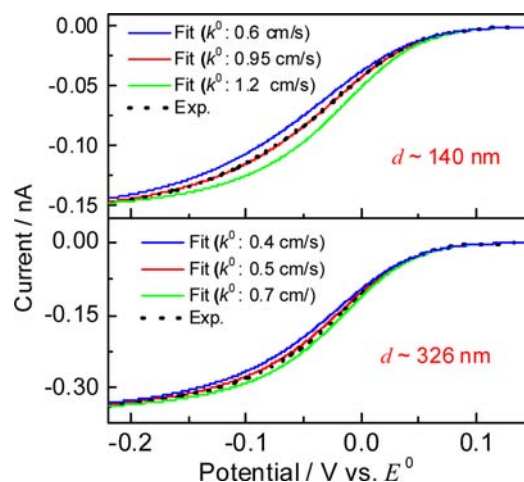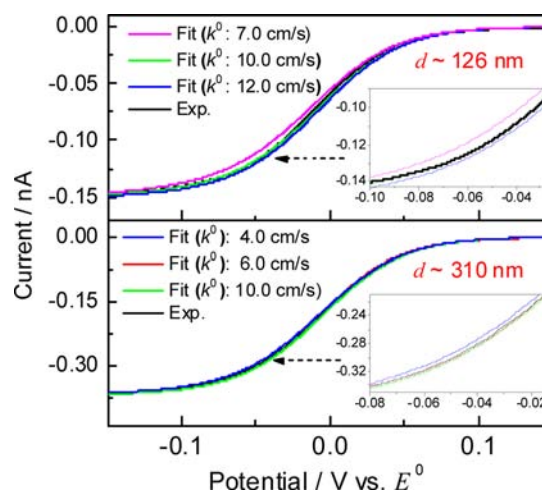

Figure 5. Fitting examples of the polarization curves obtained on graphene electrodes prepared from suspensions I ($d \approx 126$ nm) and II ($d \approx 310$ nm), respectively, for the reduction of 10 mM $Ru(NH_3)_6^{3+}$ in 1 M KCl. The insets are the enlarged plots of the region indicated by the arrows.

was subtracted. As seen in Figure 1, the CVs exhibited some hysterisis between the forward and reverse scans, probably due to the capacitance of the SAM, the defects of r-GOs and the leads. This may result in some errors and uncertainties in kinetic analysis, which, however, would not alter the general trend of the kinetics.

It can be seen that the $E_{1/2}$ became increasingly negative as the I_{dL}^* were below some small values, indicating the transition from reversible electrode processes to irreversible ones at small r-GO flakes due to increased mass transport (MT) rates, which is the prerequisite for voltammetric determination of ET kinetics.[37,38] The reversibility transition occurred at I_{dL}^* of about 0.2 and 0.04, respectively, for $Fe(CN)_6^{3-}$ and $Ru(NH_3)_6^{3+}$, indicating that the latter has much more facile ET kinetics. To gain more insights into the ET kinetics at r-GOs, the polarization curves obtained at r-GO flakes with I_{dL}^* below 0.04 (those from the suspensions I and II) were used to extract the standard rate constants (k^o) of the two redox probes through numerical fitting by using the finite-element method (FEM) under the Comsol Multiphysics package,[22] with ET kinetics described by the Butler−Volmer equation[37] and the mass transport treated by steady-state diffusion (SI, section 4).

Figures 4 and 5 each show two representative fitting examples for the reduction of $Fe(CN)_6^{3-}$ and $Ru(NH_3)_6^{3+}$, respectively. In these fittings, the r-GO flakes were modeled as disks with effective diameters of d estimated from I_{dL}^*. For each polarization curve, a range of k^o values were tested, and the best fits and those nearby are given. For electrodes prepared from r-GO suspension I, fittings were also performed with rectangle geometries of different length and width combinations (SI, section 4) and similar k^o values were obtained (Figures S6 and S7 of the SI). This should be due to the fact that the r-GO ribbons in suspension I had very low aspect ratios. The real mass transport rates therefore would not differ significantly from disks of similar sizes.

We found that the polarization curves for the reduction of $Fe(CN)_6^{3-}$, on electrodes prepared from both suspension I and suspension II, can be best fitted with a relatively unambiguous value of k^o (Figure 4). For the reduction of $Ru(NH_3)_6^{3+}$, however, only the polarization curves on electrodes prepared from r-GO suspension I can be best fitted with a relatively explicit k^o, while the polarization curves obtained on electrodes with relatively large r-GO flakes from suspension II in most cases can be fitted with a range of k^o values (Figure 5). This should be due to that the ET kinetics of $Ru(NH_3)_6^{3+}$ is too fast,

so that the electrode processes at large r-GO flakes remained considerably impacted by the MT, although some deviation from total reversibility did occur. The shifts of polarization curves from the reversible one were not pronounced (e.g., only a few mV in $E_{1/2}$). Therefore, the voltammetric analyis cannot provide an accurate value of k^o.

Figure 6 displays the lowest k^o values that can best fit the polarization curves obtained on a number of electrodes prepared from r-GO suspensions I and II for the two ET reactions. For the reduction of $Fe(CN)_6^{3-}$, most of the displayed values should represent the real values of k^o. For the reduction of $Ru(NH_3)_6^{3+}$, however, only those obtained at small r-GOs from suspension I might be reliable, whereas those at the larger flakes merely tell that the k^o was not lower than them. At the small r-GO flakes, k^o of 9−10 cm/s were typically obtained for $Ru(NH_3)_6^{3+}$. To reliably measure such fast ET kinetics, electrodes with MT coefficients (m) not less than 2 cm/s should be used so that k^o/m is not larger than 5. For an ultramicroelectrode with an effective diameter around 300 nm,
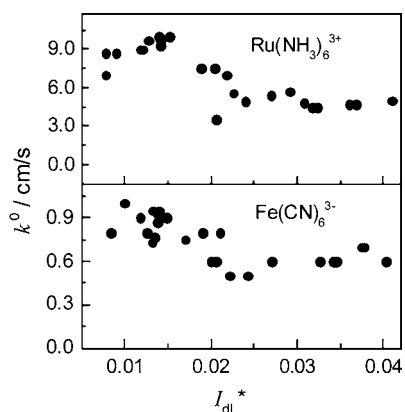
10076

dx.doi.org/10.1021/ja402456b | *J. Am. Chem. Soc.* 2013, 135, 10073−10080

Figure 6. The lowest values of k^o for the reduction of $Ru(NH_3)_6^{3+}$ and $Fe(CN)_6^{3-}$ provided by the voltammetric fittings on r-GO of various sizes.

however, the m should be around 1.0 cm/s ($m = 2D/d$, $D \approx 1 \times 10^{-5}$ cm^2/s).

An important question in the electrochemistry of graphene and other sp^2 carbons such as highly oriented pyrolytic graphite (HOPG) is the role of surface defects in their electrochemical reactivity. Recent literature on graphene has shown that the edges and defects are more reactive than the basal plane.[34] Similarly, numerous works have suggested that edge plane sites and defects are the predominant origin of electrochemical activity of HOPG.[35,36] The poor electrode kinetics on defect-free sp^2 carbon surfaces has been believed to be due to their low local density of states (DOS) near the Fermi level.[37,39] The latter can be significantly increased by introducing defects.[40]

The k^o values for the reduction of $Fe(CN)_6^{3-}$ and $Ru(NH_3)_6^{3+}$ obtained at the small r-GOs in present study were very close to those obtained on metal nanoelectrodes,[18b,19,41] and much higher than those reported for HOPG and graphenes.[34–36] Raman spectra of these small r-GOs exhibited comparable intensities between D and G bands (Figure 7 and Figures S8 and S9 of the SI, where D peak at ~1352 cm^{-1} is a defect peak due to intervalley scattering and G peak at ~1584 cm^{-1} is associated with the pristine sp^2 domains). In addition, these r-GOs also exhibited S3 peaks at 2900–2950 cm^{-1} (a second-order peak due to the D–G
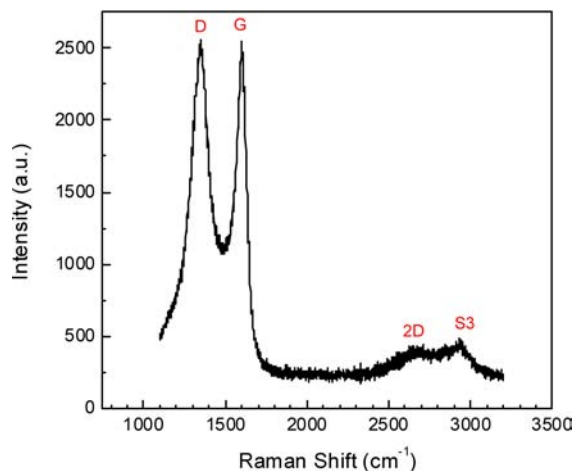
combination) with higher intensity than the 2D peaks around 2650 cm^{-1}. These Raman features indicated that the prepared r-GOs were dominated with defects,[42] which may be responsible for their high activity for heterogeneous ET reactions. It is imaginable that small r-GOs should have undergone severe oxidation, which would therefore be dominated with edges and other defects.

As shown in Figures S8 and S9 of the SI (these spectra were sampled under a lower laser power than that for Figure 7, see SI, section 2.2), the Raman D/G intensity ratios, which represent the ratios of defect sites at edges and boundaries over that in sp^2 domains, were generally higher for r-GOs from suspension I than those from suspension II, indicating an increase in the defect density in smaller r-GO flakes. Accordingly, it is interesting to note from Figure 6 that the k^o values obtained for the reduction of $Fe(CN)_6^{3-}$ at the small r-GOs from suspension I (typically in the range of 0.7–1.0 cm/s) are slightly larger than those obtained on the large r-GOs (around 0.6 cm/s). This seemingly implied that the heterogonous ET kinetics at graphene-based materials is indeed correlated with the defect density. It is worth mentioning that an earlier study by Unwin et al.[18b] using Pt nanoelectrodes also showed an apparent size effect in ET kinetics for the $Fe(CN)_6^{3-}/Fe(CN)_6^{4-}$ couple. A recent study by Unwin and co-workers[43] on HOPG surfaces has also suggested that there are some factors associated with this redox couple which could make the voltammetric analysis complicated.

3.3. Diffuse Double Layer Effect on Nanosized r-GOs.

Due to the fact that the size of an electrode dictates the domain of its electrochemical interface,[37] reducing the electrode to nanometer dimensions would result in a significant extension of the diffuse electric double layer (EDL) on the entire interface.[20–24] This may raise pronounced EDL effects on interfacial ET kinetics and MT dynamics, for example, making the electroneutrality-based treatment of electrochemical MT and the Frumkin treatment of the diffuse EDL effect[37] on ET kinetics break down. Depending on the concentration of the background electrolyte, the thickness of the diffuse EDL varies from a few angstroms to several hundreds of nanometers.[37] Therefore, the electroneutrality-based mass transport may break down at electrodes of a few nanometers when the solution is strongly supported by a background electrolyte,[22] while it could occur at electrodes up to hundreds of nanometers in dilute solutions of redox probes without supporting electrolyte.[20,21,24] On this basis, the graphene electrodes obtained from r-GO suspensions I and II can be used to verify the applicability of the electroneutrality-based MT in non-supported solution.

By investigating the steady-state voltammetric responses of graphene electrodes of different sizes for the reduction of $Ru(NH_3)_6^{3+}$ and $Fe(CN)_6^{3-}$ in the presence and absence of 1 M KCl (Figures S10 and S11 of the SI), we summarize in Figure 8 the ratios between the limiting currents in the absence and presence of the supporting electrolyte (I_L/I_{dL}), as a function of I_{dL}^*. The values of I_L/I_{dL} quantitatively describe the influence of the supporting electrolyte on the limiting transport rates of the electroactive species. By assuming an electroneutrality-based diffusion and electromigration of the electroactive species and ignoring the diffuse EDL effect, Amatore et al.[44] have derived a theoretical formula for I_L/I_{dL} (eq 1).
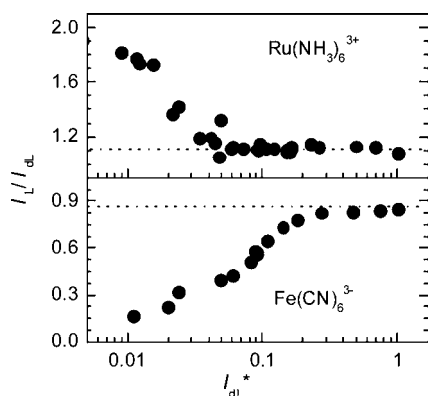

Figure 7. A representative Raman spectrum of r-GO flakes from suspension I.

10077

dx.doi.org/10.1021/ja402456b | *J. Am. Chem. Soc.* 2013, 135, 10073–10080

Figure 8. Ratios between the limiting currents for the reduction of $Ru(NH_3)_6^{3+}$ and $Fe(CN)_6^{3-}$ in the absence and presence of 1 M KCl as a function of r-GO sizes ($I_{dL}*$). The dotted lines are the ratios calculated from eq 1.

$$\frac{i_L}{i_{dL}} = 1 \pm z \left\{ 1 + (1 + |z|)\left(1 - \frac{z}{n}\right) \right.$$
$$\left. \ln\left[1 - \frac{1}{(1 + |z|)(1 - z/n)} \right] \right\} \qquad (1)$$

In eq 1, the sign ($\pm$) is positive for $n < z$ and negative for $n > z$. According to this equation, the value of I_L/I_{dL} depends only on the charge of the reactant (z) and the electron transfer number in the electrode reaction (n, positive for reduction and negative for oxidation), and is independent of electrode dimension. The validation of eq 1 has been justified by microelectrode studies of a range of redox probes, including those studied here.[44,45]

It can be seen from Figure 8 that the removal of the supporting electrolyte led to enhanced and inhibited limiting currents, respectively, for the reduction of cation ($Ru(NH_3)_6^{3+}$) and anion ($Fe(CN)_6^{3-}$). At electrodes of relatively large $I_{dL}*$, the magnitudes of the enhancement or the inhibition were all around 10% and nearly invariant with $I_{dL}*$, which agreed reasonably with the prediction of eq 1 (the dotted lines), indicating that the diffuse EDL had insignificant influence on the mass transport of the studied redox probes at the large r-GO flakes.

As $I_{dL}*$ was below some small values, the I_L/I_{dL} started to depart from the relatively constant values seen at large r-GOs. The departure occurred at an $I_{dL}*$ of ca. 0.03 and 0.2, respectively, for the reduction of $Ru(NH_3)_6^{3+}$ and $Fe(CN)_6^{3-}$, which corresponded to radii of about 150 nm and 1.0 μm, respectively, if considering the r-GOs as disks. With the decrease in r-GO size, the magnitude of the departure increased, manifesting the increased diffuse EDL effect at the electrochemical interfaces of small r-GOs.

The diffuse EDL effect seemed to be much more pronounced for the reduction of $Fe(CN)_6^{3-}$. Similar phenomena were also observed previously on Pt and carbon microelectrodes,[20a,45b,46] which has been attributed to the formation of a passivation layer through ferricyanide decomposition[45b,46a] and/or the diffuse EDL effect on the ET kinetics,[46b] i.e., the so-called Frumkin effect.[37] As seen from Figure S11 of the SI, the steady-state voltammetric responses for this probe severely lagged at small r-GO flakes in the absence of supporting electrolyte. At r-GOs of nanometer dimensions, the voltammetric currents were nearly completely

inhibited upon removal of the supporting electrolyte, which seemed to tell that there was indeed an increased inhibition of the ET kinetics as well as the MT dynamics due to the diffuse EDL at interfaces of smaller r-GOs. Since no well-defined limiting currents were established for $Fe(CN)_6^{3-}$ reduction on very small electrodes, only approximate values of I_L/I_{dL} were obtained by using the current values at the lower potential limits. For the reduction of $Ru(NH_3)_6^{3+}$, the diffuse EDL effects were only seen on the MT dynamics because that the ET kinetics are too facile so that the limiting transport occurs well before the appearance of the kinetic effect of the diffuse EDL.

3.4. Further Discussions. It should be pointed out that the values of $I_{dL}*$ may only qualitatively distinguish the sizes of different r-GO flakes, due to their irregular and varied geometries as seen from the AFM and TEM images. For instances, the short r-GO ribbons in suspension I could have differing aspect ratios, and the flakes in suspensions II more or less deviate from ideal disk shapes. Besides, we have assumed that the r-GO flakes would lay on the end surface of SAM due to the hydrophobic interaction between the graphene surface and the end surface of SAM. We believe that in most cases this should be true. In some rare cases, however, other orientation of r-GOs such as intercalation into the SAM layer and/or standing vertically on SAM surface may occur, especially for the smallest flakes. These geometry and orientation complexities would complicate the relationship between the r-GO sizes (therefore the MT rates) and the dimensionless limiting current $I_{dL}*$.

As discussed earlier, despite the irregularity and variation, the shapes of the relatively large r-GO flakes in the present study are mostly close to disk. Although the smaller flakes are more like ribbons, they have very low aspect ratios. Therefore, the mass transport rates at r-GOs in the present study should not differ significantly from disks of similar sizes, making the kinetic analysis reliable at least in qualitative trend.

In the case that an r-GO flake may stand on and/or partially intercalate into the SAM, the exposed surface areas would be doubled. As a result, the electrode would give a much larger limiting current than that expected by the geometric size of r-GO. In this case, the mass transport rate would be underestimated when using the dimensionless limiting current $I_{dL}*$. This might be the reason for the considerable data scattering in the determined k^o values at small r-GOs (Figure 6). However, this should not prevent us from gaining a qualitative trend in the k^o variation with the r-GO size.

In the case that the r-GO is fully intercalated in the SAM, the electron transfer and mass transport would be strongly inhibited. In this case, no well-defined sigmoid voltammetric responses would be obtained. In this study, we did not use such voltammetric responses for kinetic analysis.

4. CONCLUSIONS

In summary, high-temperature annealing followed by high-speed centrifugation and size-selected ultrafiltration has enabled us to separate r-GO flakes of submicrometer and nanometer sizes from the large ones. These ultrasmall flakes can be used to construct nanometer and submicrometer graphene electrodes by using SAM-modified Au electrodes of appropriately small sizes as supports to attach individual flakes in their dilute suspensions. The fabricated graphene ultramicroelectrodes can be used to study the fast heterogeneous ET kinetics at r-GOs and the nanoscopic charge transport dynamics at electrochemical interfaces.

Numerical fittings of the voltammetric responses of the fabricated graphene electrodes with nanometer-sized r-GO flakes have shown that the k^o values of $Ru(NH_3)_6^{3+}$ and $Fe(CN)_6^{3-}$ could be as high as 9–10 cm/s and 0.7–1.0 cm/s respectively, which are similar to that observed at metal electrodes but much higher than those reported at basal planes of HOPG and graphenes. The high electrochemical ET activity on these small r-GOs may be explained in terms of their defect-dominant nature, as revealed by the Raman spectroscopic results. Furthermore, an accordant increase in the Raman defect density and k^o with the decreased r-GO sizes has been observed, which seemingly further stresses the correlation between the ET activity and the defect density at carbon surfaces.

The voltammetric responses of the fabricated graphene electrodes in the absence of supporting electrolyte show enhanced and inhibited limiting transport currents for the reduction of $Ru(NH_3)_6^{3+}$ and $Fe(CN)_6^{3-}$, respectively, as expected from the coupled electromigration–diffusion transport. As the tethered r-GO flakes are of submicrometer and nanometer dimensions, however, the enhancing and/or inhibiting magnitudes significantly deviate from that predicted by the mass transport equations based on electroneutrality assumption, which may evidence the increased penetration of the diffuse EDL into the mass transport layer at nanoscopic electrochemical interfaces.

■ ASSOCIATED CONTENT

Ⓢ Supporting Information

Chemicals, apparatus, and measurements; preparation of GOs; and supporting figures. This material is available free of charge via the Internet at http://pubs.acs.org.

■ AUTHOR INFORMATION

Corresponding Author

slchen@whu.edu.cn

Notes

The authors declare no competing financial interest.

■ ACKNOWLEDGMENTS

■ REFERENCES

(1) Brownson, D. A. C.; Kampouris, D. K.; Banks, C. E. *Chem. Soc. Rev.* **2012**, *41*, 6944–6976.

(2) (a) Chlistunoff, J.; Cliffel, D.; Bard, A. J. *Thin Solid Films* **1995**, *257*, 166–184. (b) Birkett, P. R.; Taylor, R.; Wachter, N. K.; Carano, M.; Paolucci, F.; Roffia, S.; Zerbetto, F. *J. Am. Chem. Soc.* **2000**, *122*, 4209–4212.

(3) (a) Campbell, J. K.; Sun, L.; Crooks, R. M. *J. Am. Chem. Soc.* **1999**, *121*, 3779–3780. (b) Heller, I.; Kong, J.; Heering, H. A.; Williams, K. A.; Lemay, S. G.; Dekker, C. *Nano Lett.* **2005**, *5*, 137–142. (c) Nugent, J. M.; Santhanam, K. S. V.; Rubio, A.; Ajayan, P. M. *Nano Lett.* **2001**, *1*, 87–91. (d) Wang, C.; Waje, M.; Wang, X.; Tang, J. M.; Haddon, R. C.; Yan, Y. *Nano Lett.* **2004**, *4*, 345–348.

(4) (a) Zhu, Y. W.; Murali, S.; Stoller, M. D.; Ganesh, K. J.; Cai, W.; Ferreira, P. J.; Pirkle, A.; Wallace, R. M.; Cychosz, K. A.; Thommes, M.; Su, D.; Stach, E. A.; Ruoff, R. S. *Science* **2011**, *332*, 1537–1541. (b) Zhang, L. L.; Zhao, X.; Ji, H. X.; Stoller, M. D.; Lai, L. F.; Murali, S.; Mcdonnell, S.; Cleveger, B.; Wallacec, R. M.; Ruoff, R. S. *Energy Environ. Sci.* **2012**, *5*, 9618–9625. (c) Skinner, B.; Fogler, M. M.;

Shklovskii, B. I. *Phys. Rev. B* **2011**, *84*, 235133–235145. (d) Stoller, M. D.; Park, S. J.; Zhu, Y. W.; An, J. H.; Ruoff, R. S. *Nano Lett.* **2008**, *8*, 3498–3502. (e) El-Kady, M. F.; Strong, V.; Dubin, S.; Kaner, R. B. *Science* **2012**, *335*, 1326–1330.

(5) (a) Gong, K. P.; Du, F.; Xia, Z. H.; Dustock, M.; Dai, L. M. *Science* **2009**, *323*, 760–764. (b) Yu, D. S.; Nagelli, E.; Du, F.; Dai, L. M. *J. Phys. Chem. Lett.* **2010**, *1*, 2165–2173. (c) Zhang, S. M.; Zhang, H. Y.; Liu, Q.; Chen, S. L. *J. Mater. Chem. A* **2013**, *1*, 3302–3308. (d) Li, Y. G.; Zhou, W.; Wang, H. L.; Xie, L. M.; Liang, Y. Y.; Wei, F.; Idrobo, J. C.; Pennycook, S. J.; Dai, H. J. *Nat. Nanotechnol.* **2012**, *7*, 394–400.

(6) (a) Yoo, E. J.; Kim, J.; Hosono, E.; Zhou, H. S.; Kudo, T.; Honma, I. *Nano Lett.* **2008**, *8*, 2277–2282. (b) Zhou, G.; Wang, D. W.; Li, F.; Zhang, L.; Li, N.; Wu, Z. S.; Wen, L.; Lu, G. Q.; Cheng, H. M. *Chem. Mater.* **2010**, *22*, 5306–5313. (c) Wang, C.; Li, D.; Too, C. O.; Wallace, G. G. *Chem. Mater.* **2009**, *21*, 2604–2606.

(7) (a) Geim, A. K. *Science* **2009**, *19*, 1530–1534. (b) Li, X.; Cai, W.; An, J.; Kim, S.; Nah, J.; Yang, D.; Piner, R.; Velamakanni, A.; Jung, I.; Tutuc, E.; Banerjee, S. K.; Colombo, L.; Ruoff, R. S. *Science* **2009**, *5*, 1312–1314. (c) Bae, S.; Kim, H.; Lee, Y.; Xu, X.; Park, J. S.; Zheng, Y.; Balakrishnan, J.; Lei, T.; Kim, H.; Song, Y. I.; Kim, Y. J.; Kim, K. S.; Ozyilmaz, B.; Ahn, J. H.; Hong, B. H.; Iijima, S. *Nat. Nanotechnol.* **2010**, *5*, 574–578.

(8) (a) Güell, A. G.; Ebejer, N.; Snowden, M. E.; Macpherson, J. V.; Unwin, P. R. *J. Am. Chem. Soc.* **2012**, *134*, 7258–7261. (b) Xia, J.; Chen, F.; Li, J.; Tao, N. *Nat. Nanotechnol.* **2009**, *4*, 505–509. (c) Chen, F.; Qing, Q.; Xia, J.; Li, J.; Tao, N. *J. Am. Chem. Soc.* **2009**, *131*, 9908–9909.

(9) (a) Li, W. T. C.; Lowe, M. A.; Abruña, H. D.; Ralph, D. C. *ACS Nano* **2011**, *5*, 2264–2270. (b) Rodriguez-Lopez, J.; Ritzert, N. L.; Mann, J. A.; Tan, C.; Dichtel, W. R.; Abruna, H. D. *J. Am. Chem. Soc.* **2012**, *134*, 6224–6236.

(10) (a) Li, X.; Zhu, Y.; Cai, W.; Borysiak, M.; Han, B.; Chen, D.; Piner, R. D.; Colombo, L.; Ruoff, R. S. *Nano Lett.* **2009**, *9*, 4359–4363. (b) Dudin, P. V.; Snowden, M. E.; Macpherson, J. V.; Unwin, P. R. *ACS Nano* **2011**, *5*, 10017–10025.

(11) (a) Moon, I. K.; Lee, J.; Ruoff, R. S.; Lee, H. *Nat. Commun.* **2010**, *1*, 73–78. (b) Dreyer, D. R.; Park, S. J.; Bielawski, C. W.; Ruoff, R. S. *Chem. Soc. Rev.* **2010**, *39*, 228–2401.

(12) (a) Zhou, M.; Zhai, Y.; Dong, S. *Anal. Chem.* **2009**, *81*, 5603–5613. (b) Guo, S. J.; Dong, S. J. *Chem. Soc. Rev.* **2011**, *40*, 2644–2672. (c) Shan, C.; Yang, H.; Song, J.; Han, D.; Ivaska, A.; Niu, L. *Anal. Chem.* **2009**, *81*, 2378–2382.

(13) (a) Yang, S.; Xu, B.; Zhang, J.; Huang, X.; Ye, J.; Yu, C. *J. Phys. Chem. C* **2010**, *114*, 4389–4393. (b) Xie, X.; Zhao, K.; Xu, X.; Zhao, W.; Liu, S.; Zhu, Z.; Li, M.; Shi, Z.; Shao, Y. *J. Phys. Chem. C* **2010**, *114*, 14243–14250.

(14) (a) Zhou, M.; Wang, Y.; Zhai, Y.; Zhai, J.; Ren, W.; Wang, F.; Dong, S. *Chem.—Eur. J.* **2009**, *15*, 6116–6120. (b) Li, F.; Xue, M.; Ma, X.; Zhang, M.; Cao, T. *Anal. Chem.* **2011**, *83*, 6426–6430.

(15) (a) Gooding, J. J.; Ciampi, S. *Chem. Soc. Rev.* **2011**, *40*, 2704–2718. (b) Ulman, A. *Chem. Rev.* **1996**, *96*, 1533–1554.

(16) Liu, B.; Bard, A. J.; Mirkin, M. V.; Creager, S. E. *J. Am. Chem. Soc.* **2004**, *126*, 1485–1492.

(17) (a) Chazalviel, J. N.; Allongue, P. *J. Am. Chem. Soc.* **2011**, *133*, 762–764. (b) Su, L.; Gao, F.; Mao, L. *Anal. Chem.* **2006**, *78*, 2651–2657. (c) Diao, P.; Liu, Z. *J. Phys. Chem. B* **2005**, *109*, 20906–20913. (d) Kissling, G. P.; Milesa, D. O.; Fermın, D. J. *Phys. Chem. Chem. Phys.* **2011**, *13*, 21175–21185.

(18) (a) Watkins, J. J.; Chen, J. Y.; White, H. S.; Abruña, H. D.; Maisonhaute, E.; Amatore, C. *Anal. Chem.* **2003**, *75*, 3962–3971. (b) Slevin, C. J.; Gray, N. J.; Macpherson, J. V.; Webb, M. A.; Unwin, P. R. *Electrochem. Commun.* **1999**, *1*, 282–288. (c) Penner, R. M.; Heben, M. J.; Longin, T. L.; Lewis, N. S. *Science* **1990**, *250*, 1118–1121. (d) Li, Y.; Bergman, D.; Zhang, B. *Anal. Chem.* **2009**, *81*, 5496–5502.

(19) (a) Mirkin, M. V. *Isr. J. Chem.* **2010**, *50*, 291–305. (b) Sun, P.; Mirkin, M. V. *Anal. Chem.* **2006**, *78*, 6526–6534. (c) Mirkin, M. V.; Shao, Y. *Anal. Chem.* **1997**, *69*, 1627–1634.

(20) (a) Norton, J. D.; White, H. S.; Feldberg, S. W. *J. Phys. Chem.* **1990**, *94*, 6772−6780. (b) Watkins, J. J.; White, H. S. *Langmuir* **2004**, *20*, 5474−5483. (c) White, H. S. *Anal. Chem.* **2002**, *74*, 4577−4582. (d) Conyers, J. L.; White, H. S. *Anal. Chem.* **2000**, *72*, 4441−4446. (e) Smith, C. P.; White, H. S. *Anal. Chem.* **1993**, *65*, 3343−3353.

(21) (a) Chen, S. L.; Kucernak, A. *J. Phys. Chem. B* **2002**, *106*, 9396−9404. (b) Chen, S. L.; Kucernak, A. *Electrochem. Commun.* **2002**, *4*, 80−85. (c) Liu, Y. W.; Zhang, Q. F.; Chen, S. L. *Electrochim. Acta* **2010**, *27*, 8280−8286.

(22) (a) He, R.; Chen, S. L.; Yang, F.; Wu, B. L. *J. Phys. Chem. B* **2006**, *110*, 3262−3270. (b) Sun, Y.; Liu, Y. W.; Liang, Z. X.; Xiong, L.; Wang, A. L.; Chen, S. L. *J. Phys. Chem. C* **2009**, *113*, 9878−9883. (c) Liu, Y. W.; He, R.; Zhang, Q. F.; Chen, S. L. *J. Phys. Chem. C* **2010**, *114*, 10812−10822.

(23) (a) Batchelor-McAuley, C.; Dickinson, E. J. F.; Rees, N. V.; Toghill, K. E.; Compton, R. G. *Anal. Chem.* **2012**, *84*, 669−684. (b) Dickinson, E. J. F.; Compton, R. G. *J. Phys. Chem. C* **2009**, *113*, 17585−17589. (c) Henstridge, M. C.; Dickinson, E. J. F.; Compton, R. G. *Chem. Phys. Lett.* **2010**, *485*, 167−170.

(24) (a) Limon-Petersen, J. G.; Streeter, I.; Rees, N. V.; Compton, R. G. *J. Phys. Chem. C* **2009**, *113*, 333−337. (b) Streeter, I.; Compton, R. G. *J. Phys. Chem. C* **2008**, *112*, 13716−13728. (c) Limon-Petersen, J. G.; Streeter, I.; Rees, N. V.; Compton, R. G. *J. Phys. Chem. C* **2008**, *112*, 17175−17182.

(25) Sun, P.; Zhang, Z. Q.; Guo, J. D.; Shao, Y. H. *Anal. Chem.* **2001**, *73*, 5346−5351.

(26) Cox, J. T.; Zhang, B. *Annu. Rev. Anal. Chem.* **2012**, *5*, 253−272.

(27) Hummers, W. S.; Offeman, R. E. *J. Am. Chem. Soc.* **1958**, *80*, 1339−1339.

(28) (a) Stankovich, S.; Dikin, D. A.; Piner, R. D.; Kohlhaas, K. A.; Kleinhammes, A.; Jia, Y.; Wu, Y.; Nguyen, S. T.; Ruoff, R. S. *Carbon* **2007**, *45*, 1558−1565. (b) Tung, V. C.; Allen, M. J.; Yang, Y.; Kaner, R. B. *Nat. Nanotechnol.* **2009**, *4*, 25−29.

(29) (a) Li, X. L.; Wang, H. L.; Robinson, J. T.; Sanchez, H.; Diankov, G.; Dai, H. J. *J. Am. Chem. Soc.* **2009**, *131*, 15939−15944. (b) Gao, W.; Alemany, L. B.; Ci, L. J.; Ajayan, P. M. *Nat. Chem.* **2009**, *1*, 403−408. (c) Yang, D; V. A.; Bozoklu, G.; Park, S.; Stoller, M.; Piner, R. D.; Stankovich, S.; Jung, I.; Field, D. A.; Ventrice, C. A., Jr.; Ruoff, R. S. *Carbon* **2009**, *47*, 145−152.

(30) Mezour, M. A.; Morin, M.; Mauzeroll, J. *Anal. Chem.* **2011**, *83*, 2378−2382.

(31) Li, X.; Wang, X.; Zhang, L.; Lee, S.; Dai, H. *Science* **2008**, *319*, 1229−1232.

(32) (a) Lotya, M.; Hernandez, Y.; King, P. J.; Smith, R. J.; Nicolosi, V.; Karlsson, L. S.; Blighe, F. M.; De, S.; Wang, Z.; McGovern, I. T.; Duesberg, G. S.; Coleman, J. N. *J. Am. Chem. Soc.* **2009**, *131*, 3611−3620. (b) Shin, K. Y.; Hong, J. Y.; Jang, J. *Adv. Mater.* **2011**, *23*, 2113−2118.

(33) (a) He, C.; Li, Z.; Cai, M.; Cai, M.; Wang, J. Q.; Tian, Z.; Zhang, X.; Shen, P. K. *J. Mater. Chem. A* **2013**, *1*, 1401−1406. (b) Ragoussi, M. E.; Malig, J.; Katsukis, G.; Butz, B.; Spiecker, E.; de la Torre, G.; Torres, T.; Guldi, D. M. *Angew. Chem., Int. Ed.* **2012**, *51*, 6421−6425.

(34) (a) Tan, C.; Rodríguez-López, J.; Parks, J. J.; Ritzert, N. L.; Ralph, D. C.; Abruña, H. D. *ACS Nano* **2012**, *6*, 3070−3079. (b) Sharma, R.; Baik, J. H.; Perera, C. J.; Strano, M. S. *Nano Lett.* **2010**, *10*, 398−405.

(35) (a) Cline, K. K.; McDermott, M. T.; McCreery, R. L. *J. Phys. Chem.* **1994**, *98*, 5314−5319. (b) McCreery, R. L. *Chem. Rev.* **2008**, *108*, 2646−2687. (c) McDermott, M. T.; Kneten, K.; McCreery, R. L. *J. Phys. Chem.* **1992**, *96*, 3124−3130.

(36) (a) Banks, C. E.; Moore, R. R.; Davies, T. J.; Compton, R. G. *Chem. Commun.* **2004**, 1804−1805. (b) Davies, T. J.; Hyde, M. E.; Compton, R. G. *Angew. Chem.* **2005**, *44*, 5121−5126. (c) Hyde, M. E.; Davies, T. J.; Compton, R. G. *Angew. Chem., Int. Ed.* **2005**, *44*, 6491−6496. (d) Ji, X. B.; Buzzeo, M. C.; Banks, C. E.; Compton, R. G. *Electroanalysis* **2006**, *18*, 44−52. (e) Banks, C. E.; Davies, T. J.; Wildgoose, G. G.; Compton, R. G. *Chem. Commun.* **2005**, 829−841.

(37) Bard, A. J.; Faulkner, L. R. *Electrochemical Methods: Fundamentals and Applications*, 2nd ed.; Wiley: New York, 2001.

(38) (a) Mirkin, M. V.; Bard, A .J . *Anal. Chem.* **1992**, *64*, 2293−2302. (b) Oldham, K. B.; Zoski, , C. G. *J. Electroanal. Chem.* **1988**, *256*, 11−19. (c) Oldham, K. B. *Steady State Voltammetry. In Microelectrode: Theory and Application*; Montenegro, M. I., Queiros, M. A., Daschbach, J. L., Eds.; Kluwer: Dordrecht, The Netherlands, 1991; pp 35−50.

(39) (a) McCreery, R. L.; McDermott, M. T. *Anal. Chem.* **2012**, *84*, 2602−2605. (b) Royea, W. J.; Hamann, T. W.; Brunschwig, B. S.; Lewis, N. S. *J. Phys. Chem. B* **2006**, *110*, 19433−19442. (c) Gerischer, H.; McIntyre, R.; Scherson, D.; Storck, W. *J. Phys. Chem.* **1987**, *91*, 1930.

(40) (a) Ugeda, M. M.; Brihuega, I.; Guinea, F.; Gomez-Rodriguez, J. M. *Phys. Rev. Lett.* **2010**, *104*, 096804−096807. (b) Schweitzer, L. *Phys. Rev. B* **2009**, *80*, 245430−245435.

(41) (a) Wang, C.; Hu, X. *Talanta* **2006**, *68*, 1322−1328. (b) Velmurugan, J.; Sun, P.; Mirkin, M. V. *J. Phys. Chem. C* **2009**, *113*, 459−464.

(42) Wang, H. L.; Robinson, J. T.; Li, X. L.; Dai, H. J. *J. Am. Chem. Soc.* **2009**, *131*, 9910−9911.

(43) (a) Patel, A. N.; Collignon, M. G.; O'Connell, M. A.; Hung, W. O. Y.; McKelvey, K.; Macpherson, J. V.; Unwin, P. R. *J. Am. Chem. Soc.* **2012**, *134*, 20117−20130. (b) Lai, S. C. S.; Patel, A. N.; McKelvey, K.; Unwin, P. R. *Angew. Chem., Int. Ed.* **2012**, *51*, 1−5.

(44) (a) Amatore, C.; Fosset, B. *J. Electroanal. Chem.* **1988**, *256*, 255−268. (b) Amatore, C.; Deakin, M. R.; Wightman, R. M. *J. Electroanal. Chem.* **1987**, *220*, 49−63.

(45) (a) Ciszkowska, M.; Jaworski, A.; Osteryoung, J. G. *J. Electroanal. Chem.* **1997**, *423*, 95−101. (b) Lee, C.; Anson, F. C. *J. Electroanal. Chem.* **1992**, *323*, 381−389.

(46) (a) Beriet, C.; Pletcher, D. *J. Electroanal. Chem.* **1993**, *361*, 93−101. (b) Rooney, M. B.; Coomber, D. C.; Bond, A. M. *Anal. Chem.* **2000**, *72*, 3486−3491.